

Article

Numerical Simulation Analysis of Difference from a Radial Resistivity Testing Method for Cylindrical Cores and a Conventional Testing Method

Jiahuan He ^{1,2,3,*}, Tangyan Liu ¹, Long Wen ^{2,3}, Tingting He ², Min Li ⁴, Jin Li ^{2,3}, Li Wang ^{2,3} and Xin Yao ^{2,3}¹ School of Ocean and Earth Science, Tongji University, Shanghai 200092, China² Exploration and Development Research Institute, PetroChina Southwest Oil & Gasfield Company, Chengdu 610041, China³ Shale Gas Evaluation and Exploitation Key Laboratory of Sichuan Province, Chengdu 610213, China⁴ State Key Laboratory of Oil and Gas Reservoir Geology and Exploitation, Southwest Petroleum University, Chengdu 610500, China

* Correspondence: hejiahuan@petrochina.com.cn; Tel.: +86-28-8560-4341

Abstract: Rock resistivity is a major geophysical technical parameter in geological and geotechnical engineering, geothermal prospecting, and oil and gas exploration. Its accurate measurement is of great significance to achieve the goal of “carbon peak and carbon neutrality”. To solve anisotropic problems, a method to test the radial resistivity in cylindrical core samples has been proposed and has been deemed the universal method, as it has the virtues of no specially processed sample being needed and nondestructive testing. However, there is still a difference in the radial resistivities obtained from this method and another testing method that is commonly used for cuboid samples. Furthermore, the differences between these methods have not yet been made clear in China or elsewhere. Therefore, we compared the results of the above-two testing methods via numerical simulations after establishing the potential field distribution, and, in combination with their methodological principles, illustrated the differences between the resistivities determined in samples with distinct shapes obtained using the two testing methods, summarized the conditions when there was zero difference and considerable difference when using the two methods, and provided a theoretical basis for the reasonable selection of an appropriate method to test the resistivity anisotropy.

Keywords: complex variable function; anisotropy; rock resistivity; radial resistivity

MSC: 86-10



Citation: He, J.; Liu, T.; Wen, L.; He, T.; Li, M.; Li, J.; Wang, L.; Yao, X. Numerical Simulation Analysis of Difference from a Radial Resistivity Testing Method for Cylindrical Cores and a Conventional Testing Method. *Mathematics* **2022**, *10*, 2885. <https://doi.org/10.3390/math10162885>

Academic Editor: Maria Alessandra Ragusa

Received: 4 July 2022

Accepted: 6 August 2022

Published: 12 August 2022

Publisher's Note: MDPI stays neutral with regard to jurisdictional claims in published maps and institutional affiliations.



Copyright: © 2022 by the authors. Licensee MDPI, Basel, Switzerland. This article is an open access article distributed under the terms and conditions of the Creative Commons Attribution (CC BY) license (<https://creativecommons.org/licenses/by/4.0/>).

1. Introduction

In 2008, the UN Intergovernmental Panel on Climate Change (IPCC) set the goal of “carbon neutrality” to prevent the global average temperature from rising by more than 1.5 °C by the end of the current century [1–7]. The consumption of fossil fuels is the main source of carbon dioxide. To adapt to this new situation, oil consumption will continue to grow in the short to middle terms and will then ultimately return to its nature of being a “basic raw material”. Many existing oil and gas companies, including PetroChina, are already focusing on developing technologies for new energy resources, such as wind power, solar power, electrical energy, and hydrogen energy. However, different from other energy companies, oil and gas companies have the advantage of having access to subsurface resources that are currently available. Natural gas, the only fossil energy with increased use during the carbon-neutrality stage, will be the best partner for new energy resources for a long time to come. As for geothermal energy, another kind of new energy, the exploitation technologies are highly similar to those used for oil and gas.

Figuring out the physical properties of the fluid flowing in rocks has been an ongoing task in the history of “carbon peak and carbon neutrality”. Clearly, the rock resistivity

discussed in this paper is a physical property. With a powerful meaning in geophysics, it is a vital parameter in the exploration domain that can be used to evaluate oil and gas reservoirs, especially for reservoir classification, fluid distribution determination, and reserve calculation [8–12]. Moreover, it helps geophysicists interpret and determine seismic and volcanic activities as well as large tectonic events [13–16]. Moreover, resistivity is a critical physical parameter in geological and geotechnical engineering, geothermal prospecting, and oil and gas exploration [17–20]. Therefore, obtaining an accurate and representative resistivity parameter is vital to achieving the goal of “carbon peak and carbon neutrality” as soon as possible.

Anisotropy, one of the greatest problems experienced when acquiring accurate rock resistivity measures [21–23], is also a universal physical property in common materials or media. Moreover, there is often a big anisotropic difference among crystals, various materials used in daily life, and earth media. The international geophysical community is well aware of the importance of anisotropy among physical properties [24–26]. Geophysicists once concentrated their attention on the anisotropy of thermal conductivity in rocks [27]. Jan Safanda (1995) [28] used a numerical solution to express the effects of thermal conductivity anisotropy by building a 2D anisotropy model of rocks in the geothermal field. Both David Deming (1994) [29] and Pribnow (1995) [30] set up experimental approaches to test the thermal conductivity in both cuttings and core samples at room temperature. Resistivity anisotropy is similar to thermal conductivity anisotropy. Due to their very long geological history, the sedimentation, diagenesis, and tectonism joint affecting oil and gas reservoirs may lead to reservoirs having anisotropy and different resistivity values in various directions.

For the sake of clarifying resistivity anisotropy, some scholars (including Tao Zhu, 2009 [31]; Bin Zhang, 2015 [32], 2017 [14]; Chaoqiang Fang, 2018 [33]; Qiuming Gong, 2017 [34]; and Jinzhen An, 1996 [35]) have measured anisotropy by preparing cuboid samples using diamond wire slicing or direct cutting. It is evident that the cores obtained from drilling directly are unable meet the requirements of the above methods and that the most common cores are cylindrical in shape.

2. Problem Statement

Unlike cuboid samples, it is impossible to calculate the resistivity of cylindrical samples directly. As such, in 2020, Jiahuan He et al. established a new method to test radial resistivity [36] and applied the theory of complex variable function to build a mathematical model to determine anisotropic resistivity. This new method has solved technical problems that previous methods could not determine, such as the radial resistivity of cylindrical samples. This method has been successfully applied to characterize the resistivity anisotropy in shale, sandstone, and vuggy carbonate reservoirs, which may support effective natural gas exploration and development in Sichuan Basin, China.

Figure 1a shows a rather simple experimental device that this new method (Jiahuan He, 2020 [36]) uses to test the radial resistivity of cylindrical samples, which are very common in the oil and gas domain. This method is widely useful for anisotropy characterization. As shown in Figure 1b,c, the radial resistivity is derived from $\rho = K/K'$ LR by fully attaching a curved electrode to the sample sidewall at a specific angle after conformal transformation as well as after Schwartz–Christoffel transformation, where in $K(\alpha) = \int_0^1 \frac{dt}{\sqrt{(1-t^2)(1-\alpha^2 t^2)}}$.

It is unnecessary to restate that this method is better for solving the radial resistivity than conventional ones. However, several scholars have also pointed that when using the radial resistivity testing method, the basis for using the complex variable function is that the cores are assumed to be isotropic. However, the final results that are derived actually illustrate that they are anisotropic. Meanwhile, all of the real cylindrical cores are three-dimensional, while the two-dimensional complex variable function is adopted in this method, which also implies an assumption that the properties of the cores vary uniformly in the axial direction. Therefore, it is necessary to compare the two results individually

from the radial resistivity testing method and the conventional resistivity anisotropy testing method used for cubic samples.

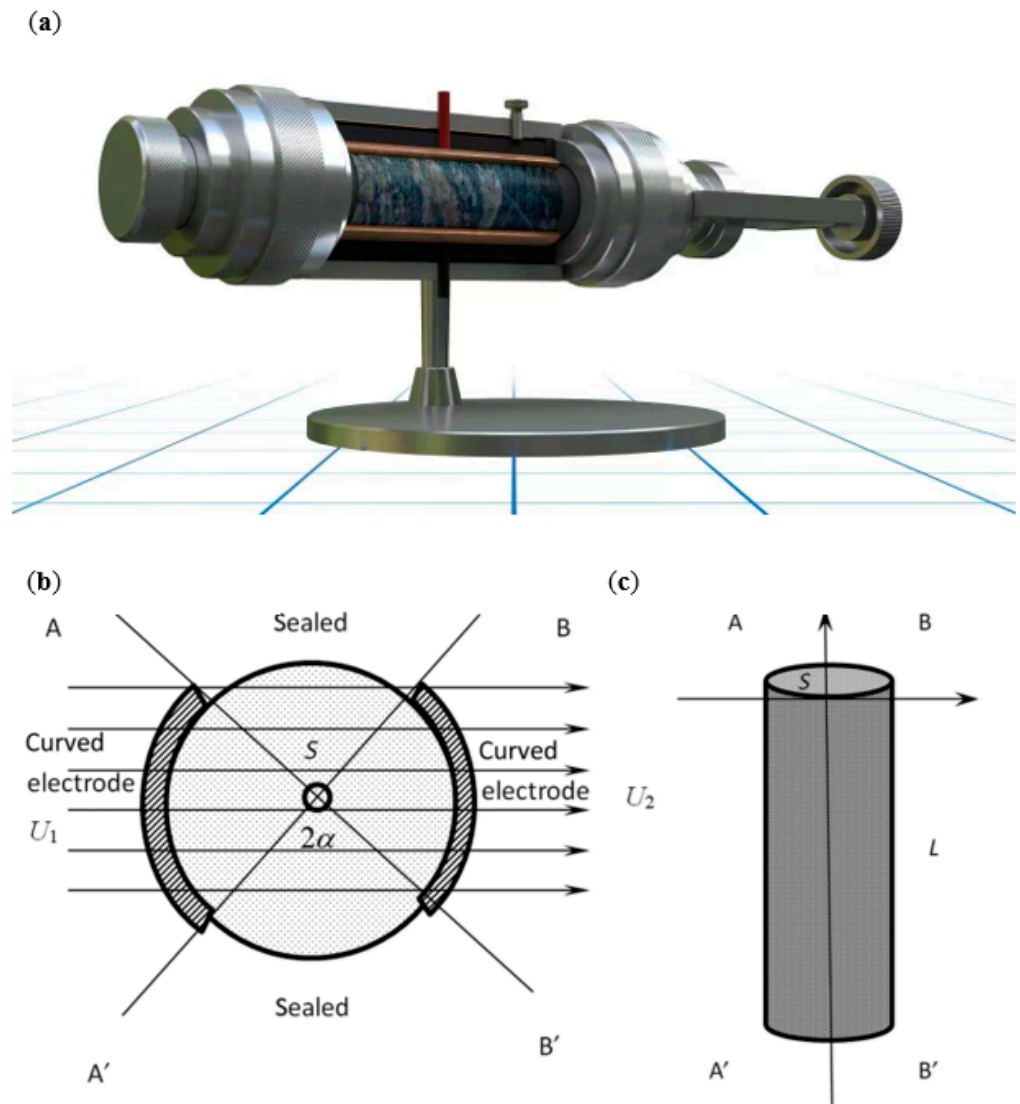


Figure 1. Radial resistivity testing method: (a) experimental device; (b) top view of cylindrical core; (c) cylindrical core.

3. Methodology

In order to define the effectiveness of the radial resistivity testing method, a finite element numerical simulation approach was used for various samples to analyze each testing error. Previously, cube samples were used for anisotropy testing. Thus, in this testing process, all of the experiments were simulated using the numerical simulation approach. An experimental resistivity result on one cuboid numerical sample was first obtained to act as a benchmark; then, the radial resistivity of another cylindrical numerical sample with the same property was simulated; finally, the discrepancy between the two resistivities resulting from the cuboid and cylindrical samples individually was analyzed.

According to the potential field theory, the potential field distribution in the reservoir rocks can be described by the following equations:

$$\nabla \cdot J = Q_{j,v} \quad (1)$$

$$J = \sigma E + J_e \quad (2)$$

$$E = -\nabla U \quad (3)$$

In the 3D cuboid coordinate system, the current density is as follows:

$$J = iJ_x + jJ_y + kJ_z \quad (4)$$

The divergence of the current density is expressed as follows:

$$\nabla \cdot J = \partial J_x / \partial x + \partial J_y / \partial y + \partial J_z / \partial z \quad (5)$$

The electric field intensity is defined as follows:

$$E = iE_x + jE_y + kE_z \quad (6)$$

Equation (7) describes the 3D vector value of the differential operator:

$$\nabla = i\partial/\partial x + j\partial/\partial y + k\partial/\partial z \quad (7)$$

Using COMSOL Multiphysics Simulation software, the potential field distribution was obtained using finite element numerical simulation. The testing was carried out from the left ends to the right ends of the samples. For the cylindrical samples, the radial resistivity from the left end to the right end was tested using a curved electrode with a centering angle of $\pi/2$. Figure 2 shows the current direction. The yellow arrow in the figure represents the current flowing from the positive electrode to the negative electrode.

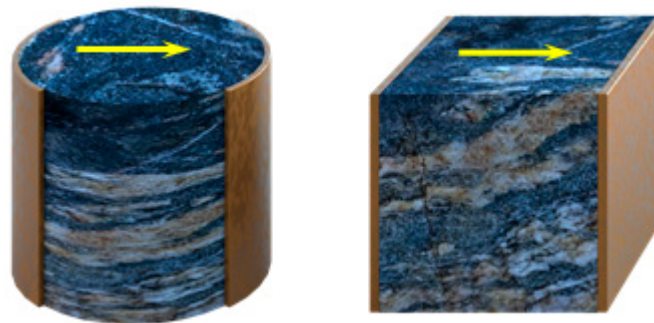


Figure 2. Current direction simulated using radial resistivity testing method.

Based on the radial resistivity testing method proposed by Jianhuan He (2020 [36]), the measured resistivity value was calculated using the electrical charges across the electrode per unit time under the known potential difference.

Equation (8) expresses the potential difference between both sample ends.

$$U_{ab} = \iiint_{\Sigma} E dv / S \quad (8)$$

Equation (9) formulates the current passing through the electrode.

$$I_y = \iint_S J_y ds / l \quad (9)$$

Relatively, the conductivity is as follows:

$$\rho = R \frac{S}{l} = \frac{U_{ab}}{\iint_S J_y ds / l} \frac{S}{l} = \frac{U_{ab} S}{\iint_S J_y ds} \quad (10)$$

Equation (11) explains the resistivity of the cube sample.

$$\rho_{\text{cube}} = \frac{U_{ab}l}{I} \quad (11)$$

Equation (12) illustrates the radial resistivity of the cylindrical sample.

$$\rho_{\text{cylinder}} = \frac{U_{ab}S}{\iint_S J_y ds} \quad (12)$$

Most of the objects in the real world have very complex anisotropy. To simplify computation, three extremes covering both lamination development and the testing direction in the samples were considered first, as shown in Figure 3.

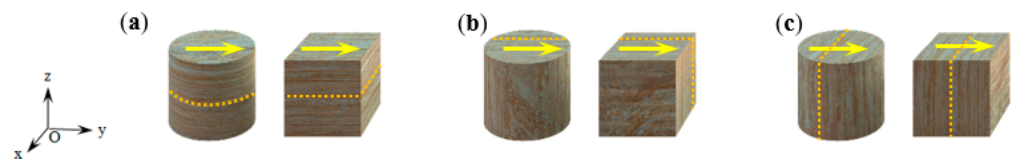


Figure 3. Radial resistivity testing method corresponding to three extremes. The arrow represents the current direction during the test, and the dotted line represents the lamination direction of the rock. θ is an included angle between the lamination plane and the end, and φ is an included angle between the projection of the lamination plane on the end and the current direction: (a) Extreme 1: $\theta = 0$, $\varphi = 0$; (b) Extreme 2: $\theta = \pi/2$, $\varphi = 0$; (c) Extreme 3: $\theta = \pi/2$, $\varphi = \pi/2$.

Moderate voltage was at first imposed on both ends of the samples in the three extremes. Additionally, corresponding potential fields were then generated after the numerical simulation. Next, the resistivity of the cuboid sample and the radial resistivity of the cylindrical sample were calculated. Finally, after contrasting these two resistivities, a systematic error that appeared during radial resistivity testing was analyzed.

4. Numerical Simulation Results

To reflect the error obtained during the radial resistivity testing corresponding to the three extremes above more clearly, additional simulations were performed for two kinds of materials with resistivities of 1:10 and by supposing that the resistivities of material 1 and material 2 were $1 \Omega \text{ m}$ and $10 \Omega \text{ m}$, respectively. The three extremes were simulated one by one. For convenience of contrast, the cross-section of the cylindrical sample on the zOx plane mentioned below was the same as that of the cube (a special cuboid) sample, and the end-circle diameter of the cylindrical sample was equal to the side length of the cube sample. Since the resistivity testing method used for the cube sample was one that is traditionally adopted to evaluate resistivity anisotropy, the testing results were taken as the denominator of the relative error between the two during later calculations. For the cylindrical sample, h_i and $D-h_i$ represented the lengths of the two line segments that passed through the center of the cross-section of the cylindrical end, and they were perpendicular to the interface between the two materials and separated by the material interface in the i th instance. For the cube sample, h_i and $D-h_i$ represented the thicknesses of the two materials separated by the interface in the i th instance.

4.1. Extreme 1

Supposing that the sample consisted of double-deck materials with different resistivities, the thicknesses were denoted as h_1 and $D-h_1$ for upper material 1 and lower material 2, respectively. The potential field distribution could be simplified to a cross-sectional 2D model to implement one numerical simulation because the sample resistivities were equivalent at the same Z -axis. Obviously, for both the cylindrical and cube samples, another numerical simulation was carried out using the same drawing at the cross-section on the

zOx plane. The two simulation results were bound to be identical. Thus, for the radial resistivity in Extreme 1, the systematic error was 0.

4.2. Extreme 2

Supposing that the interface of the double-deck materials used in the sample was parallel to not only the zOy plane but also the current direction, and the thicknesses were denoted as h_2 and $D-h_2$ for material 1 and material 2, respectively, as shown in Figure 4. Because both cylindrical and cube samples had the same property at the same Z-axis, the model could be simplified to the projected drawing at the cross-section on the xOy plane for the numerical simulation.

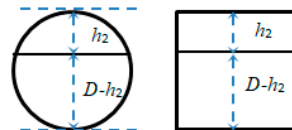
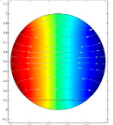
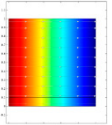
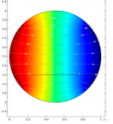
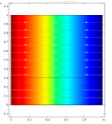
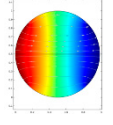
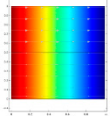
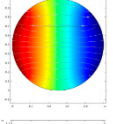
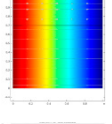
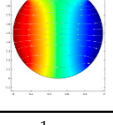
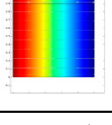


Figure 4. Extreme 2: different material thicknesses.

Some of results from the numerical simulation can be found in Table 1. The maximum difference between the two testing methods appeared in the low-resistivity materials at the current edge because, in the radial resistivity testing method, the curved electrode failed to touch these materials, while the electrode in the cube testing electrode always touched them. As such, in Extreme 2, there was a relative difference between the two testing results. In other extremes, the difference was less than 11%. However, the results from the two testing methods were identical, and the error was zero when the double-deck materials maintained a 50–50 split.

Table 1. Extreme 2: numerical simulation results of different material thicknesses.

h_2	$D-h_2$	Potential Field Distribution from Radial Testing	Resistivity Simulated by Radial Testing ($\Omega \text{ m}$)	Potential Field Distribution from Cube Testing	Resistivity Simulated by Cube Testing ($\Omega \text{ m}$)	Systematic Error ¹ (%)
0.9	0.1		1.036		1.099	−5.73
0.7	0.3		1.315		1.340	−1.87
0.5	0.5		1.818		1.818	0.00
0.3	0.7		2.994		2.703	10.77
0.1	0.9		9.008		5.263	71.16

¹ Here, systematic error refers to the difference between the radial resistivity testing value and the cube sample testing value divided by the latter value.

4.3. Extreme 3

Supposing that the interface of the double-deck materials was parallel to not only the xOz plane but also the current direction, the thicknesses were denoted as h_3 and $D-h_3$ for material 1 and material 2, respectively, as shown in Figure 5. Because the cylindrical and cube samples both had the same property at the same Z-axis, the model could be simplified to the projected drawing at the cross-section on the xOy plane for the numerical simulation.

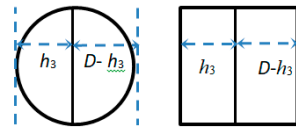


Figure 5. Extreme 3: different material thicknesses.

Some of the experimental results from the numerical simulation are listed in Table 2. The radial resistivity testing results differed from the other testing results obtained from the cube samples the most when the vertical direction of the current was located at one end for a few high-resistivity materials. This is because, in radial resistivity testing, both ends of the curved electrode make direct contact with the low-resistivity materials, resulting in that part of the current flowing directly from one electrode end to another end through these low-resistivity materials; however, during cube testing, the current first had to pass through the high-resistivity materials before flowing from one electrode end to another end. In the other extremes, the difference in the resistivity between the two testing methods was less than 3%. As a matter of fact, there are still several transitional cases among these three extremes, which are discussed as below.

Table 2. Extreme 3: numerical simulation results of different material thicknesses.

h_3	$D-h_3$		Potential Field Distribution from Radial Testing	Resistivity Simulated by Radial Testing ($\Omega \cdot m$)	Potential Field Distribution from Cube Testing	Resistivity Simulated by Cube Testing ($\Omega \cdot m$)	Systematic Error (%)
0.9	0.1			1.116		1.900	−41.26
0.7	0.3			3.603		3.700	−2.62
0.5	0.5			5.514		5.500	0.25
0.3	0.7			7.276		7.300	−0.33
0.1	0.9			9.319		9.100	2.41

4.4. Transitional Case 1 (from Extreme 2 to Extreme 3)

In Transitional Case 1, the case in which there was a transition from Extreme 2 to Extreme 3, there was a specific included angle between the two directions of lamination

development and current, and the sample was homogeneous in the Z direction. It is easy to see from Table 3 that regardless of the included angle, the results from the two testing methods did not exceed 8% when the ratio of the low-resistivity materials to high-resistivity ones was 50/50. In the event that the two kinds of materials occupied different areas, large significant differences were only observed between the two testing methods when a small amount of high-resistivity materials was in the cylindrical end face or a when a few low-resistivity ones were on the sample margin parallel to the current direction; otherwise, the significant difference was no more than 10%.

Table 3. Transitional Case 1: numerical simulation results of different material thicknesses.

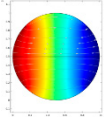
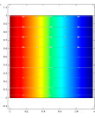
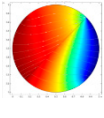
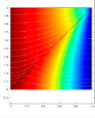
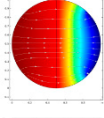
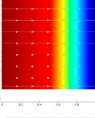
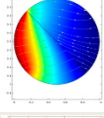
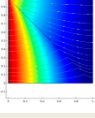
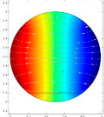
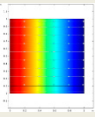
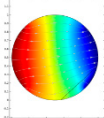
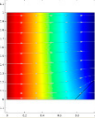
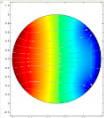
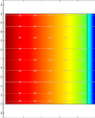
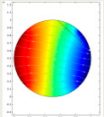
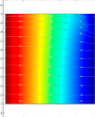
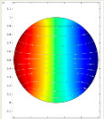
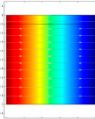
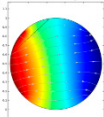
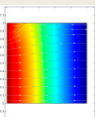
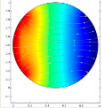
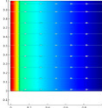
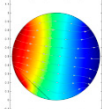
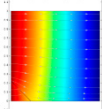
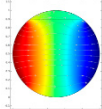
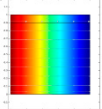
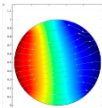
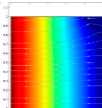
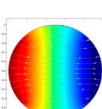
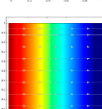
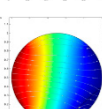
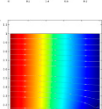
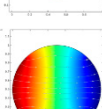
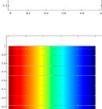
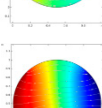
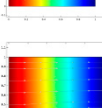
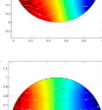
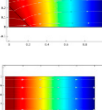
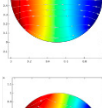
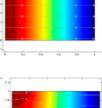
h_4	$D-h_4$	Angle between Lamination and Y-axis	Potential Field Distribution from Radial Testing	Resistivity Simulated by Radial Testing (Ω m)	Potential Field Distribution from Cube Testing	Resistivity Simulated by Cube Testing (Ω m)	Systematic Error (%)
0.5	0.5	0°		1.818		1.818	0.00
0.5	0.5	45°		2.989		3.099	−3.55
0.5	0.5	90°		5.514		5.500	0.25
0.5	0.5	135°		3.532		3.836	−7.93
0.9	0.1	0°		1.036		1.099	−5.73
0.9	0.1	45°		1.142		1.044	9.39
0.9	0.1	90°		1.117		1.900	−41.21
0.9	0.1	135°		1.141		1.043	9.40
0.9	0.1	180°		1.036		1.099	−5.73
0.9	0.1	225°		1.101		1.062	3.67

Table 3. Cont.

h_4	$D-h_4$	Angle between Lamination and Y-axis	Potential Field Distribution from Radial Testing	Resistivity Simulated by Radial Testing (Ω m)	Potential Field Distribution from Cube Testing	Resistivity Simulated by Cube Testing (Ω m)	Systematic Error (%)
0.9	0.1	270°		1.283		1.900	−32.47
0.9	0.1	315°		1.099		1.064	3.29
0.1	0.9	0°		9.008		5.263	71.16
0.1	0.9	45°		8.707		9.579	−9.10
0.1	0.9	90°		9.053		9.100	−0.52
0.1	0.9	135°		8.718		9.579	−8.99
0.1	0.9	180°		9.050		5.263	71.96
0.1	0.9	225°		9.299		9.563	−2.76
0.1	0.9	270°		9.969		9.100	9.55
0.1	0.9	315°		9.323		9.569	−2.57

4.5. Transitional Case 2 (from Extreme 1 to Extreme 2 and from Extreme 1 to Extreme 3)

As listed in Tables 4 and 5, Transitional Case 2, which included one subtransition from Extreme 1 to Extreme 2 and another from Extreme 1 to Extreme 3, was studied via numerical simulation. Since these two subtransitions could not project certain overlapping current lines, interfaces, or the uniform electric field distribution on the same plane, only 3D numerical simulation was adopted for the calculation.

Table 4. Transitional Case 2 (one subtransition from Extreme 1 to Extreme 2): numerical simulation results of different material thicknesses.

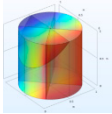
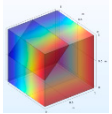
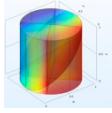
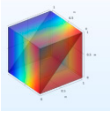
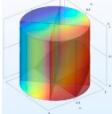
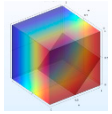
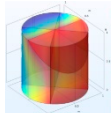
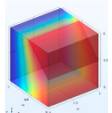
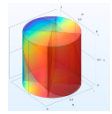
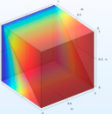
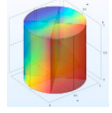
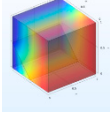
h_5	$D-h_5$	Potential Field Distribution from Radial Testing	Resistivity Simulated by Radial Testing (Ω m)	Potential Field Distribution from Cube Testing	Resistivity Simulated by Cube Testing (Ω m)	Systematic Error (%)
0.25	0.75		5.233		8.247	−36.55
0.5	0.5		2.100		1.818	15.51
0.75	0.25		1.115		1.127	−1.07

Table 5. Transitional Case 2 (another subtransition from Extreme 1 to Extreme 3): numerical simulation results of different material thicknesses.

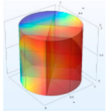
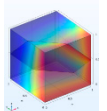
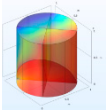
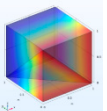
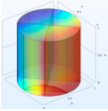
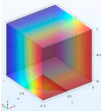
h_6	$D-h_6$	Potential Field Distribution from Radial Testing	Resistivity Simulated by Radial Testing (Ω m)	Potential Field Distribution from Cube Testing	Resistivity Simulated by Cube Testing (Ω m)	Systematic Error (%)
0.25	0.75		8.270		8.034	2.94
0.5	0.5		2.599		3.851	−32.51
0.75	0.25		1.261		1.270	−0.71

As listed in Table 4, for the subtransition from Extreme 1 to Extreme 2, there was a bigger difference between the two when there was a higher proportion of high-resistivity materials. As listed in Table 5, when both high-resistivity and low-resistivity materials accounted for half of the samples, there was a bigger difference between the two. However, a small difference often was often observed in other extremes and cases.

4.6. Transitional Case 3 (Transition from Extreme 1, Extreme 2, and Extreme 3)

As for Transitional Case 3, the numerical simulation could only be realized in 3D space. As listed in Table 6, when the low-resistivity materials were present in a low proportion, there was a difference of nearly 40% between the two testing results. Nevertheless, there was very little difference when there was an increase in the materials.

Table 6. Transitional Case 3 (transition from Extreme 1, Extreme 2, and Extreme 3): numerical simulation results of different material thicknesses.

h_7	$D-h_7$	Potential Field Distribution from Radial Testing	Resistivity Simulated by Radial Testing ($\Omega \text{ m}$)	Potential Field Distribution from Cube Testing	Resistivity Simulated by Cube Testing ($\Omega \text{ m}$)	Systematic Error (%)
0.25	0.75		2.506		4.160	−39.76
0.5	0.5		1.254		1.267	1.02
0.75	0.25		1.034		1.028	0.58

The numerical simulations on the above extremes and cases show that (1) there was no difference between the results of the two testing methods for Extreme 1; (2) for Extreme 2, the difference was less than 11%, with the exception of a small amount of low-resistivity materials at the current edge when there was a big difference between the two; (3) for Extreme 3, the difference was less than 3%, with the exception of when the vertical current direction of a few high-resistivity materials was at one end; and (4) for the three transitional cases, a considerable difference was observed, but the two testing results were in good agreement when the low-resistivity materials made the largest contribution.

As such, the radial resistivity testing results and the results of other tests used for the cube samples were similar as long as the lamination and current directions of the tested samples were perpendicular and parallel to each other or when small amounts of materials with very different properties did not appear at the sample edge. Extreme 1 was ideal because the two testing results were identical, and the theoretical error was zero.

5. Discussion

Both similarity and difference were observed in the testing results from the cylindrical and cube samples, which constitute two kinds of materials with different resistivities, as discussed above. Next, it is necessary to further consider exceptional circumstances and to analyze the main factors affecting the difference between these results.

5.1. Effects on Resistivity When Double-Deck Materials Feature Various Resistivity Differences

As per the above analysis, in Extreme 2, there was a great deal of difference between the two test methods when only a small number of low-resistivity materials were located at the current edge. One special circumstance with a bigger difference was chosen to set the scope of the resistivity difference from big (1:10) to small (1:1). As listed in Table 7, when the resistivity difference was less than 1:2, the two differed by just 6.66%. As listed in Table 8, when the quantity of low-resistivity materials at the current edge increased to some extent, the systematic error was only a little more than 10%, even though the resistivity difference was up to 1:10.

Table 7. Numerical simulation results for resistivity difference in various materials (0.1:0.9).

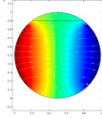
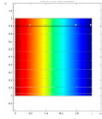
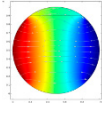
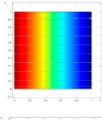
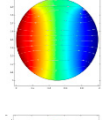
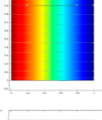
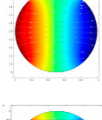
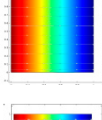
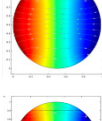
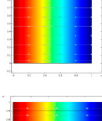
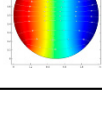
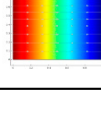
ρ_1	ρ_2	Potential Field Distribution from Radial Testing	Resistivity Simulated by Radial Testing (Ω m)	Potential Field Distribution from Cube Testing	Resistivity Simulated by Cube Testing (Ω m)	Systematic Error (%)
1	10		9.008		5.263	71.16
1	8		7.281		4.706	54.72
1	6		5.508		4.000	37.70
1	4		3.772		3.077	22.59
1	2		1.939		1.818	6.66
1	1		1.000		1.000	0

Table 8. Numerical simulation results for resistivity difference in various materials (0.3:0.7).

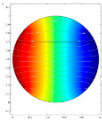
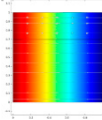
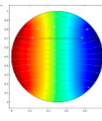
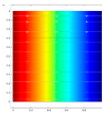
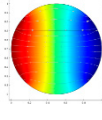
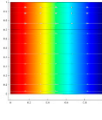
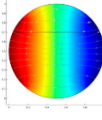
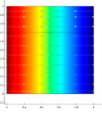
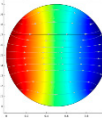
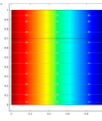
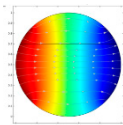
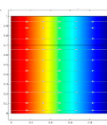
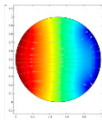
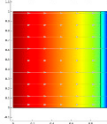
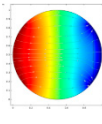
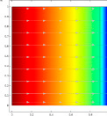
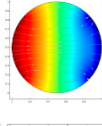
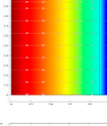
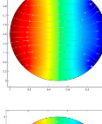
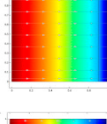
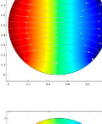
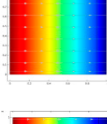
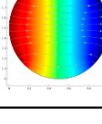
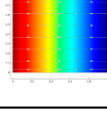
ρ_1	ρ_2	Potential Field Distribution from Radial Testing	Resistivity Simulated by Radial Testing (Ω m)	Potential Field Distribution from Cube Testing	Resistivity Simulated by Cube Testing (Ω m)	Systematic Error (%)
1	10		2.994		2.703	10.77
1	8		2.852		2.581	10.50
1	6		2.625		2.400	9.38
1	4		2.261		2.105	7.41
1	2		1.587		1.538	3.19

Table 8. Cont.

ρ_1	ρ_2	Potential Field Distribution from Radial Testing	Resistivity Simulated by Radial Testing (Ω m)	Potential Field Distribution from Cube Testing	Resistivity Simulated by Cube Testing (Ω m)	Systematic Error (%)
1	1		1.000		1.000	0

In Extreme 3, the radial resistivity test results differed from those of the cube testing method the most when the vertical current direction of a few high-resistivity materials was at one end. As listed in Table 9, the difference between the two dropped to 6.55% when the resistivity difference fell to 1:2, and a very considerable difference was observed at resistivity differences above 1:2. In other words, it should be noticed that in the actual measurements, the results from the two testing methods were not identical in terms of physical meaning.

Table 9. Extreme 3: numerical simulation results for resistivity difference in various materials (0.9:0.1).

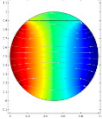
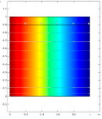
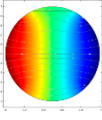
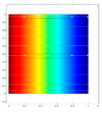
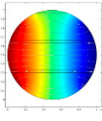
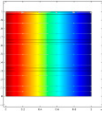
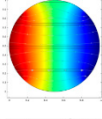
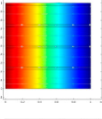
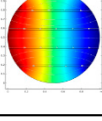
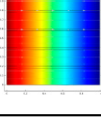
ρ_1	ρ_2	Potential Field Distribution from Radial Testing	Resistivity Simulated by Radial Testing (Ω m)	Potential Field Distribution from Cube Testing	Resistivity Simulated by Cube Testing (Ω m)	Systematic Error (%)
1	10		1.116		1.900	−41.26
1	8		1.105		1.700	−35.00
1	6		1.090		1.500	−27.33
1	4		1.067		1.300	−17.02
1	2		1.028		1.100	6.55
1	1		1.000		1.000	0

5.2. Effects of Resistivity Testing Results When the Layers of Double-Deck Materials Vary from Less to More in Proportion

To estimate whether the number of material layers affected the test results, an additional numerical simulation was targeted at Extreme 2, where the number of layers increased from higher to lower. As shown from Table 10, the difference between the two testing results decreased step by step as this number increased to a certain level, and the

systematic error was less than 10% for both materials as long as they constituted six or more layers.

Table 10. Numerical simulation results of resistivity difference in various materials (0.1:0.9).

Number of Material Layers	Potential Field Distribution from Radial Testing	Resistivity Simulated by Radial Testing (Ω m)	Potential Field Distribution from Cube Testing	Resistivity Simulated by Cube Testing (Ω m)	Systematic Error (%)
2		9.008		5.263	71.16
4		6.437		5.263	22.30
6		5.753		5.263	9.31
8		5.345		5.263	1.56
10		5.066		5.263	−3.74

5.3. Resistivity in the Sample Developed with One Fracture (with Saturated Water, without Saturated Water, and Different Fracture Angles)

It is assumed that individually, the resistivity was 1 Ω m for the fracture with 100% saturated brine, 2 Ω m for that with 50% saturated brine, and 4 Ω m for 25% saturated brine. Meanwhile, the matrix resistivity and the fracture width were set to 10 Ω m and 0.001 m. From the numerical simulation results listed in Table 11, it is not difficult to observe that the systematic error is no less than 6% for the sample developed with one fracture.

Table 11. Numerical simulation results when fractures are developed.

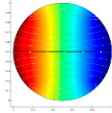
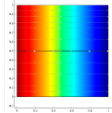
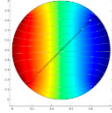
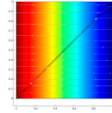
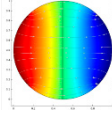
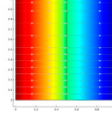
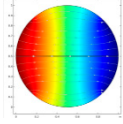
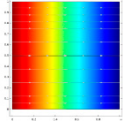
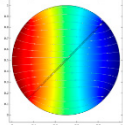
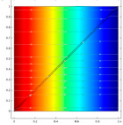
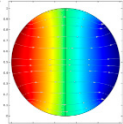
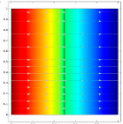
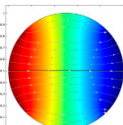
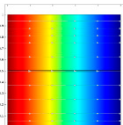
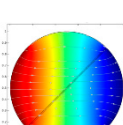
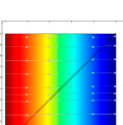
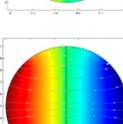
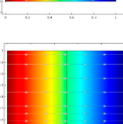
Fracture Condition	Included Angle with Current Direction	Potential Field Distribution from Radial Testing	Resistivity Simulated by Radial Testing (Ω m)	Potential Field Distribution from Cube Testing	Resistivity Simulated by Cube Testing (Ω m)	Systematic Error (%)
100% saturated brine	0°		9.596		9.175	4.59
	45°		9.329		9.578	−2.60
	90°		9.924		9.910	0.14

Table 11. Cont.

Fracture Condition	Included Angle with Current Direction	Potential Field Distribution from Radial Testing	Resistivity Simulated by Radial Testing (Ω m)	Potential Field Distribution from Cube Testing	Resistivity Simulated by Cube Testing (Ω m)	Systematic Error (%)
50% saturated brine	0°		9.860		9.615	2.55
	45°		9.319		9.788	−4.79
	90°		9.933		9.921	0.12
25% saturated brine	0°		9.948		9.852	0.97
	45°		9.369		9.912	−5.48
	90°		9.954		9.940	0.14

6. Conclusions

1. For core samples in various extremes and cases, we used numerical methods to simulate the difference between the radial resistivity test results in the cylindrical samples and the resistivity testing results in the cube samples and proved that in most extremes and cases, the agreement between the two was within the allowable error range. The cylindrical radial resistivity testing method was also confirmed to be universal and comparable to other methods that have used before. Additionally, it is an important tool for anisotropy characterization.
2. The numerical simulation results illustrate that the radial resistivity testing results in cylindrical samples were in high agreement with those obtained in cuboid samples (zero error) when the current direction was perfectly consistent with the lamination plane of the rocks.
3. The difference between the results obtained from the two testing methods was no more than 10% in most of the tested extremes and cases when the lamination plane was parallel to the current plane, with the exception of Extreme 2 and Extreme 3. When there is a small number of low-resistivity materials at the sample edge and when the interface of the different materials was parallel to the current direction (Extreme 2), the difference between the two testing results was big. The curved electrode used during radial resistivity testing failed to touch these materials, and the results were somewhat different from the test results obtained from the cube samples when the materials were

in contact with the electrode end. Moreover, there was a considerable difference when the interface between two kinds of materials was parallel to the current directions (Extreme 3). A small amount of high-resistivity materials was distributed on one end, and during radial resistivity testing, it was possible for the curved electrode to make contact with the low-resistivity materials, but during cube sample testing, the electrode only touched the high-resistivity materials representing the reason for the difference.

4. Therefore, the radial resistivity testing results and the cube sample test results are comparable as long as two extra-large systematic errors and certain special circumstances can be avoided in transitional cases during testing. In these special circumstances, the reason why the systematic error is large is that these circumstances have different physical meanings that require a more appropriate testing method to be selected according to concrete testing purposes.

Author Contributions: Conceptualization: J.H., T.L., L.W. (Long Wen) and M.L.; methodology: J.H.; software, J.H. and J.L.; validation: J.H., T.H., L.W. (Long Wen) and X.Y.; formal analysis: T.H.; investigation: J.H., T.L., L.W. (Long Wen) and M.L.; resources: L.W. (Long Wen) and L.W. (Li Wang); data curation: X.Y.; writing—original draft preparation: J.H. and T.H.; writing—review and editing: T.H.; visualization: T.H.; supervision: T.H.; project administration: J.H.; funding acquisition: J.H. All authors have read and agreed to the published version of the manuscript.

Funding: This work was supported by special funds for local science and technology development fund guided by the central government of Sichuan Province (No. 2020ZYD062).

Data Availability Statement: Data are available from the corresponding author upon reasonable request.

Acknowledgments: The authors would like to thank Zhou Keming, Zeng Li, Li Nong, Tang Zhijuan, Liu Tingzhi, and Zou Mengwen for their experiments, guidance, and suggestions. Without their assistance, this paper would not have been possible.

Conflicts of Interest: The authors declare that there are no conflict of interest regarding the publication of this paper.

References

1. Zou, C.; Xiong, B.; Xue, H.; Zheng, D.; Ge, Z.; Wang, Y.; Jiang, L.; Pan, S.; Wu, S. The role of new energy in carbon neutral. *Pet. Explor. Dev.* **2021**, *48*, 480–491. [\[CrossRef\]](#)
2. Zou, C.; Xue, H.; Xiong, B.; Zhang, G.; Pan, S.; Jia, C.; Wang, Y.; Ma, F.; Sun, Q.; Guan, C.; et al. Connotation, innovation and vision of “carbon neutral”. *Nat. Gas Ind.* **2021**, *41*, 46–57.
3. Zhou, S.; Zhu, J. Exploration of ways to helping “Carbon Peak and Neutrality” Strategy. *Nat. Gas Ind.* **2021**, *41*, 1–8.
4. Soeder, D.J. Greenhouse gas sources and mitigation strategies from a geosciences perspective. *Adv. Geo-Energy Res.* **2021**, *5*, 274–285. [\[CrossRef\]](#)
5. Li, B.; Zhu, L.; Wang, W.; Xiong, B.; Jiang, L.; Hu, R.; Mei, Q. Integrated development strategy of natural gas and hydropower in Sichuan-Chongqing area. *Nat. Gas Ind.* **2021**, *41*, 136–143.
6. Chen, J.; Li, Q.; He, J. Regional diversity of low-carbon efficiency in Sichuan province under the goal of carbon neutrality. *Nat. Gas Ind.* **2021**, *41*, 162–170.
7. Liu, F.; Qin, L.; Deng, X.; Ge, L. Progress of VSP logging technology in Sichuan Basin. *Nat. Gas Explorat. Dev.* **2020**, *43*, 39–46.
8. He, J.; Li, M.; Zhou, K.; Yang, Y.; Xie, B.; Li, N.; Dang, L.; Tang, Y. Effects of vugs on resistivity of vuggy carbonate reservoirs. *Pet. Explor. Dev.* **2020**, *47*, 527–535. [\[CrossRef\]](#)
9. Tian, H.; Xin, Y.; Zhang, H.; Wang, X.; Sun, H. Identification of complex lithology based on conventional well logging: An example from T₂I₄³ gas reservoirs, Longgang area, Sichuan Basin. *Nat. Gas Explor. Dev.* **2019**, *42*, 55–65.
10. Hou, M.; Pan, S.; Liu, H. World energy trend and China’s oil and gas sustainable development strategies. *Nat. Gas Indust.* **2021**, *41*, 9–16.
11. Wang, Y.; Xie, B.; Lai, Q.; He, X.; Yang, M.; Zhao, A.; Peng, X.; Han, B.; Bai, L. Petrophysical characteristics of deep dolomite reservoirs with and well-logging evaluation methods. *Nat. Gas Explor. Dev.* **2021**, *44*, 63–70.
12. Luo, Q.; Li, J.; Lei, X.; Xu, Q.; Dai, B.; Ma, W.; Qin, W.; Yuan, Z. Deep earth fluids: Basic characteristics and energy effects. *Nat. Gas Explor. Dev.* **2021**, *44*, 1–8.
13. Chen, F.; An, J.; Liao, C. Directional characteristic of resistivity changes in rock of original resistivity anisotropy. *Chin. J. Geophys.* **2003**, *46*, 271–280. [\[CrossRef\]](#)

14. Zhang, B.; Zhu, T.; Zhou, J. Experimental studies on the changes of rock resistivity image and anisotropy. *Acta Seismol. Sin.* **2017**, *39*, 478–494.
15. Pavel, B.; Edward, F. New interpretation of the reduction phenomenon in the electrical resistivity of rock masses before local earthquakes. *Phys. Earth Planet. Inter.* **2019**, *294*, 106279.
16. Luo, N.; Zhang, J.; Li, J.; Xin, S. Development and utilization prospect of the geothermal resources in the buried hills of the Xiong'an New Area and its periphery. *Nat. Gas Ind.* **2021**, *41*, 160–171.
17. Wang, C.; Xu, Y.; Gao, X. Rock resistivity characteristics and its application in coal mine goaf exploration. *Coal Eng.* **2020**, *52*, 64–69.
18. Jesus, G.; Jean-Christophe, C.; Anatoly, L.; Ulrich, O.; David, H. Quantification of groundwater storage heterogeneity in weathered/fractured basement rock aquifers using electrical resistivity tomography: Sensitivity and uncertainty associated with petrophysical modelling. *J. Hydrol.* **2021**, *593*, 125637.
19. Zhang, S.; Wang, Y.; Tong, Y.; Chen, Y.; Li, Z.; Niu, D. Flexural toughness characteristics of basalt fiber reinforced shotcrete composites in high geothermal environment. *Constr. Build. Mater.* **2021**, *298*, 123893. [[CrossRef](#)]
20. Kayode, J.; Adelusi, A.; Nawawi, M.; Bawallah, M.; Olowafe, T. Geo-electrical investigation of near surface conductive structures suitable for groundwater accumulation in a resistive crystalline basement environment: A Extreme study of Isuada, southwestern Nigeria. *J. Afr. Earth Sci.* **2016**, *119*, 289–302. [[CrossRef](#)]
21. Sergey, K.; Ekaterina, P.; Irina, A.; Vitaliy, D.; Elena, D.; Denis, S.; Konstantin, B. Mathematical Model of Electrical Conductivity of Anisotropic Nanocomposite with Periodic Structure. *Mathematics* **2021**, *9*, 2948.
22. Wang, F.; Xie, X.; Dong, L. Anomalous Areas Detection in Rocks Using Time-Difference. Adjoint Tomography. *Mathematics* **2022**, *10*, 1069. [[CrossRef](#)]
23. Panja, P.; McLennan, J.; Green, S. Impact of permeability heterogeneity on geothermal battery energy storage. *Adv. Geo-Energy Res.* **2021**, *5*, 127–138. [[CrossRef](#)]
24. Cao, Q.; Fang, C.; Li, Y.; Wang, H.; Fang, Q.; Shi, X. Development status of geothermal reinjection at home and abroad and its enlightenment. *Oil Drill. Prod. Technol.* **2021**, *43*, 203–211.
25. Zhan, H.; Dong, W.; Chen, S.; Hu, D.; Zhou, H.; Luo, J. Improved test method for convection heat transfer characteristics of carbonate fractures after acidizing etching. *Adv. Geo-Energy Res.* **2021**, *5*, 376–385. [[CrossRef](#)]
26. Emil N., M.; Sergey P., R.; Nail G., M. Hierarchical Approach to Identifying Fluid Flow Models in a Heterogeneous Porous Medium. *Mathematics* **2021**, *9*, 3289.
27. Yu, G.; Liu, C.; Zhang, L.; Fang, L. Parameter sensitivity and economic analyses of an interchange-fracture enhanced geothermal system. *Adv. Geo-Energy Res.* **2021**, *5*, 166–180. [[CrossRef](#)]
28. Šafanda, J. Effect of thermal conductivity anisotropy of rocks on the subsurface temperature field. *Geophys. J. Int.* **2010**, *120*, 323–330. [[CrossRef](#)]
29. David, D. Estimation of the thermal conductivity anisotropy of rock with application to the determination of terrestrial heat flow. *J. Geophys. Res.* **1994**, *99*, 22087–22091.
30. Daniel, F.; John, H. Determination of thermal conductivity for deep boreholes. *J. Geophys. Res. Solid Earth* **1995**, *100*, 9981–9984.
31. Zhu, T.; Zhou, J.; Hao, J. Resistivity anisotropy and its applications to earthquake research. *Prog. Geophys.* **2009**, *24*, 871–878.
32. Zhang, B.; Zhou, J. The experimental study on rock resistivity. *CT Theory Appl.* **2015**, *24*, 239–249.
33. Fang, C.; Li, X.; Wang, J.; Cai, C.; Cai, C. Rock physical parameters of coal reservoir in the south of Qinshui Basin. *Well Logging Technol.* **2018**, *42*, 73–77.
34. Gong, Q.; Zhou, X.; Yin, L.; He, G.; Miao, C. Study of rock breaking efficiency of TBM disc cutter based on chips analysis of linear cutting test. *Tunn. Constr.* **2017**, *37*, 363–368.
35. An, J.; Xiu, J.; Chen, F.; Chen, D. Anisotropy studies of rock resistivity changes under pressure and water replenishment. *Earthq. Res. China* **1996**, *12*, 300–306.
36. He, J.; Li, M.; Zhou, K.; Zeng, L.; Li, N.; Yang, Y.; Xiao, D.; Huang, M. Radial resistivity measurement method for cylindrical core samples. *Interpretation* **2020**, *8*, 1071–1080. [[CrossRef](#)]